DMD-Based Anti-Strong-Light Detecting and Imaging System

Zuo Tang , Xiaoheng Wang , Yefei Mao , Ruochen Zhao , Baozhen Zhao , Huicong Chang , Chang Yang , Lin Xiao *

Posted Date: 11 March 2026

doi: 10.20944/preprints202603.0912.v1

Keywords: digital micromirror device (DMD); strong light suppression; optical design; detecting and imaging system

 doi:10.20944/preprints202603.0912.v1

Article

DMD-Based Anti-Strong-Light Detecting and Imaging System

Zuo Tang, Xiaoheng Wang, Yefei Mao, Ruochen Zhao, Baozhen Zhao, Huicong Chang, Chang Yang and Lin Xiao *

China Academy of Aerospace System and Innovation, Beijing 100048, China

* Correspondence: xiaolin_82@163.com

Abstract

Strong light interference severely degrades imaging system performance. This paper presents a novel Digital Micromirror Device (DMD)-based imaging system for robust strong light suppression and long-distance detection. Our design strategically places the DMD at the primary image plane, utilizing a large F-number objective for extended depth of field. The relay imaging system employs a tilted image plane in a near-symmetric configuration to effectively balance DMD-induced aberrations, simplifying alignment and achieving a compact, high-performance layout. The DMD's regional flipping capability enables precise, dynamic suppression of strong light. Experimental results from a fabricated prototype demonstrate superior imaging quality (MTF > 0.3 at 167.3 lp/mm) and exceptional suppression of intense laser interference, ensuring clear image acquisition in challenging lighting. This system offers an efficient solution for high-quality, long-range imaging in strong light environments.

Keywords: digital micromirror device (DMD); strong light suppression; optical design; detecting and imaging system

1. Introduction

Imaging systems are indispensable in a myriad of advanced applications, including autonomous driving, medical diagnostics, industrial inspection, and surveillance, where high sensitivity, rapid response, and precision are paramount. However, the performance of these critical systems is frequently compromised by the presence of strong light interference, such as laser dazzling, intense specular reflections, or direct sunlight exposure. Such interference can lead to sensor saturation, blooming artifacts, and severe degradation of image quality, rendering the captured data unreliable or unusable for subsequent analysis and decision-making [1–5]. The ability to maintain clear and accurate imaging under these challenging conditions is thus a persistent and significant engineering challenge.

To mitigate the adverse effects of strong light interference, researchers have explored both passive and active strategies. Passive techniques often involve optical limiting materials, such as linear [6,7], nonlinear [8,9], and phase-change materials [10–12], which typically demand high excitation thresholds and often suffer from irreversible degradation or limited dynamic range under prolonged strong illumination [13,14]. Active methods, on the other hand, include mechanical shutters and spatial light modulators (SLMs). Mechanical shutters can effectively block incident light above a certain intensity, but they operate globally and do not enhance image quality in localized glare conditions [15]. Conventional SLMs, particularly those based on liquid crystal technology, offer variable attenuation but are often plagued by low light efficiency (typically below 42% with liquid crystal on silicon (LCOS) technology) and introduce phase distortions due to birefringence, especially problematic in broadband imaging applications [16–19]. These limitations underscore the need for more efficient and precise light modulation techniques.

 doi:10.20944/preprints202603.0912.v1

Digital Micromirror Devices (DMDs) have emerged as a promising alternative for pixel-level light field modulation due to their high efficiency, rapid switching speed, and precise spatial control [20,21]. Existing DMD-based systems have demonstrated capabilities in strong light suppression. For instance, Zhou et al. proposed a relay imaging system employing off-axis and tilt strategies for aberration correction [22]. However, their work, and many other existing systems, often struggle to simultaneously achieve high image quality and robust long-range detection capabilities. Ritt et al. developed a laser interference suppression method integrating three-channel band compensation with DMDs, showing effectiveness in various environments [23]. Nevertheless, this approach suffered from inadequate channel separation, leading to incomplete suppression. Subsequent work by Ritt et al. introduced a dual-channel camera system with optical multi-band components to improve channel separation; however, the inherent complexity and the DMD's flipping mechanism still resulted in signal loss within the interference band, often causing imaging distortion [24]. These prior efforts highlight the ongoing challenge in developing a DMD-based system that offers both high optical performance and effective, distortion-free strong light mitigation across a broad range of applications.

This study addresses these limitations by presenting the design of a novel anti-strong light detection and imaging system based on a DMD, featuring an optimized relay imaging configuration. Our system strategically positions the DMD at the primary image plane, with the detector at the secondary image plane, ensuring a direct and precise pixel-level mapping. For long-distance detection and imaging, the objective imaging system is designed with a long focal length and a large F-number, providing an extensive depth of field. A key aspect of our design lies in the relay imaging system, which employs a near-symmetric configuration with a tilted image plane. This innovative approach effectively compensates for the unique aberrations introduced by the DMD in a convergent light path, a significant improvement over conventional off-axis designs by simplifying alignment and adjustment, leading to a more compact layout and superior aberration control. The regional flipping capability of the DMD is then leveraged to dynamically steer strong light away from the sensor by switching affected micromirrors to –12° from their normal +12° state, thereby achieving precise and localized strong light suppression. The optical path is further folded using mirrors to achieve a compact system footprint. Simulation results demonstrate the system's high image quality, achieving a modulation transfer function (MTF) of 0.3 at 167.3 lp/mm, with maximum field curvature and distortion well-controlled at 0.11 mm and 0.64%, respectively. Experimental results with a fabricated prototype confirm both the good imaging performance and the effective suppression of strong light interference.

2. Optical Design

2.1. System Configuration and Working Principle

The operational principle of the system is illustrated in Figure 1. The detection and imaging system consists of an objective imaging assembly, a relay imaging group, a detector, a control unit, and a series of reflectors. It functions within a two-stage imaging configuration, where the DMD acts as the primary image plane, and the detector serves as the secondary image plane, maintaining precise pixel-level mapping between the two.

In operation, incident light first traverses the front objective group, converging onto the DMD's focal plane to form an intermediate image. After being reflected by the DMD, the light beam is relayed through the relaying system to the focal plane of the detector to achieve secondary imaging. Reflectors are strategically positioned to fold the optical path, enhancing the system's compactness without compromising optical performance. The control system comprises an FPGA and a DMD control board, which are respectively used for image processing, generating mask patterns, and sending instructions to control the deflection of the DMD, by adjusting the tilt angles of individual DMD mirrors to achieve high-precision spatial light modulation.

 doi:10.20944/preprints202603.0912.v1

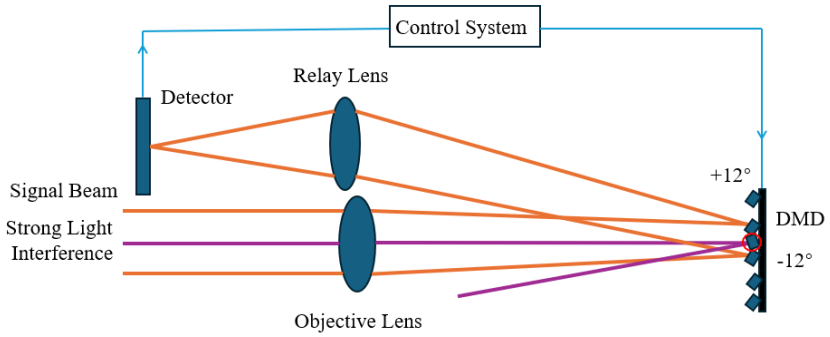

Figure 1. Working principle of the imaging system.

2.2. Detector Parameters and Determination of Focal Length

For an imaging system, the F-number typically ranges from 3 to 5. For larger depth of field (DOF) of whole system, thereby enhancing the imaging performance of the system when capturing images at long distances, the F-number of this system is set to 5. Meanwhile, based on practical applications, the system's field of view (FOV) is ±4.6 degrees. The focal length f can be calculated by the Equation (1):

$$f = h / 2 \tan \omega \tag{1}$$

where h is the diagonal length of detector, ω denotes the magnitude of the half-angle of the field of view. Since the system utilizes an IMX490 detector with dimensions of 8.69 mm × 5.63 mm and a diagonal length of 10.36 mm. System focal length calculated as 81.6mm, since F number is 5, clear aperture is 16.3mm.

2.3. Objective Imaging System Design

The objective imaging system is responsible for collecting light from the scene and forming a primary image onto the DMD. The magnification of the relay system is determined by the DMD size and detector size, is 0.6, which in turn determines that the focal length of the front-end system is 136.5 mm and its F-number is 8.5. For objective imaging system, the DOF is essential for maintaining sharp focus over a wide range of object distances, a critical requirement for long-range surveillance and detection applications. To realize a large F-number, the back focal length of the entire system has been increased. The resulting optical layout of objective imaging system is depicted in Figure 2, and the corresponding key parameters are summarized in Table 1.

Table 1. Key parameters of Objective Imaging System.

Parameters	Data
F#	8.5
Focal Length	136.5 mm
DMD Size	0.7inch（17.78 mm）
DMD Micromirror Size	13.68 μm
DMD Resolution	1920 × 1080
MTF	37 lp ≥ 0.5

In the design process of the system, it is essential to prevent light that has not been reflected by the DMD (as reflective component) from entering the relay optical system prematurely. For the present system, this requirement is specifically manifested in the necessity of increasing the distance between the DMD and the first optical mirror of the relay optical system. This is achieved by carefully optimizing the angle of incidence onto the DMD and the subsequent reflection angle. As shown in

 doi:10.20944/preprints202603.0912.v1

Figure 3, when the distance between the first optical mirror of the relay optical system and the DMD surface is 80mm or larger than 80mm, the relevant requirements will be met.

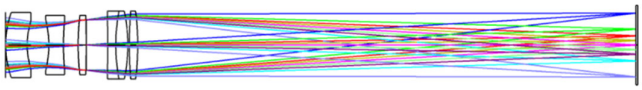

Figure 2. Schematic diagram of the Objective Imaging System.

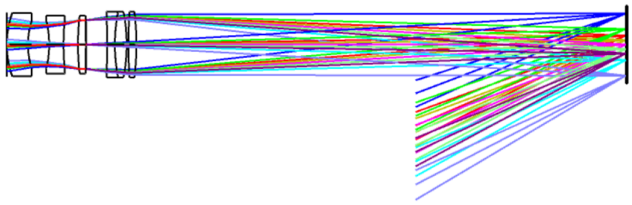

Figure 3. Schematic diagram of DMD reflection optical path.

The image quality of the objective imaging system is evaluated using the Modulation Transfer Function (MTF). As shown in Figure 4, the MTF of the objective imaging system exceeds 0.7 at 40 lp/mm and clings closely to the diffraction limit, which satisfies the design requirements.

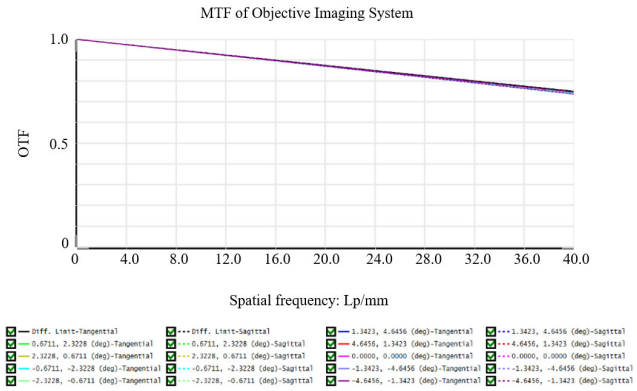

Figure 4. MTF of Objective Imaging System.

2.4. Relay System Design

The relay system's primary function is to re-image the light modulated by the DMD onto the detector, while also correcting for aberrations introduced by the preceding optical elements, especially those flipping from the DMD. A significant challenge in integrating DMD into imaging systems, especially in convergent light paths, is the introduction of aberrations due to the non-planar nature of the DMD's active surface and the angular deflection of its micromirrors. Traditional off-axis designs often lead to increased complexity of the system and introduce significant off-axis aberrations.

When light reflects off the tilted micromirrors of the DMD, it effectively creates a virtual tilted object plane for the subsequent relay system. Consequently, within the rotational plane defined by the reflected and incident optical axes, optical path differences arise between the light beams passing through different micromirrors [25], As shown in Figure 5. By tilting the detector plane at a specific angle relative to the optical axis, we can effectively compensate for the field-dependent aberrations, particularly astigmatism and field curvature, that are inherently introduced by the DMD's operation. So the relay system design here is the implementation of a near-symmetric configuration with a deliberately tilted image plane for aberration balancing rather than traditionally off-axis configuration. The layout of the optical system is shown in Figure 6, and the key parameters of the relay optical system are summarized in Table 2.

 doi:10.20944/preprints202603.0912.v1

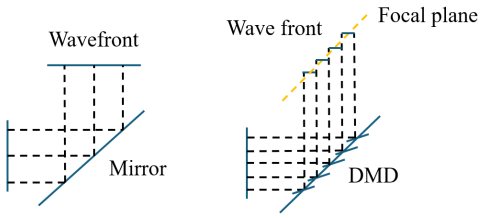

Figure 5. Schematic diagram of the DMD aberration.

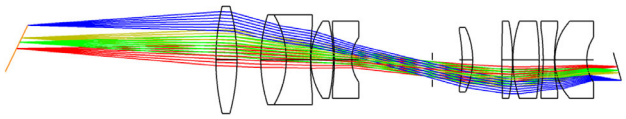

Figure 6. Schematic diagram of the relay optical system.

Table 2. Key parameters of the relay optical system.

Parameters	Data
Lateral magnification	0.22
CMOS size	8.69 mm × 5.69 mm
CMOS pixel size	3 μm × 3 μm
CMOS resolution	2880 × 1860
NA	0.04

3. Results

3.1. Overall Evaluation

The key parameters of the relay optical system are summarized in Table 3. To facilitate optimizing the whole system, the objective imaging system and the relay optical system were first integrated, followed by independent optimization of the relay system. The optical path was then folded to create the final anti-strong light detection and imaging system, as illustrated in Figure 7.

When the imaging system is used for normal imaging, its operating state is as shown in Figure 7, all micromirrors are deflected by +12°, focusing all incoming light onto the detector's focal plane to form a clear image as shown in Figure 7 (**a**). Conversely, when all micromirrors deflect by –12°, as shown in Figure 7 (**b**), all light is reflected away from the detector, preventing any light from entering the detection system. Both the front objective and the relay lenses are aligned parallel to the optical axis without tilt, which simplifies the assembly and calibration processes.

The MTF was used to evaluate the imaging resolution of the system. Based on the detector pixel size, the Nyquist frequency is calculated to be 167.3 lp/mm. The MTF curve of the optical system is presented in Figure 8. It is evident that the MTF values across the entire field of view are close to the diffraction limit, with a value of 0.3 at 167.3 lp/mm, indicating excellent imaging performance.

 doi:10.20944/preprints202603.0912.v1

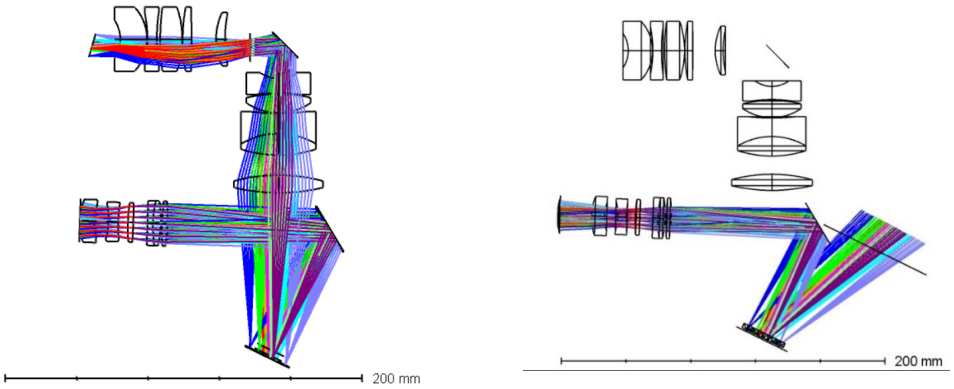

(**a**) (**b**)

Figure 7. Schematic diagram of the imaging system: (**a**) All micromirror +12°; (**b**) All micromirror -12°.

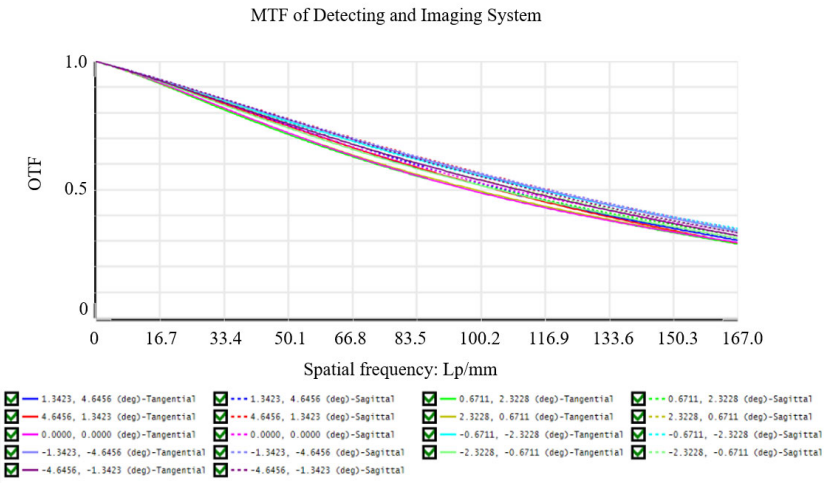

Figure 8. MTF of the imaging system.

The relative illumination of the detection and imaging system is shown in Figure 9. The illumination remains near unity over the entire field, demonstrating high and uniform imaging brightness on the detector.

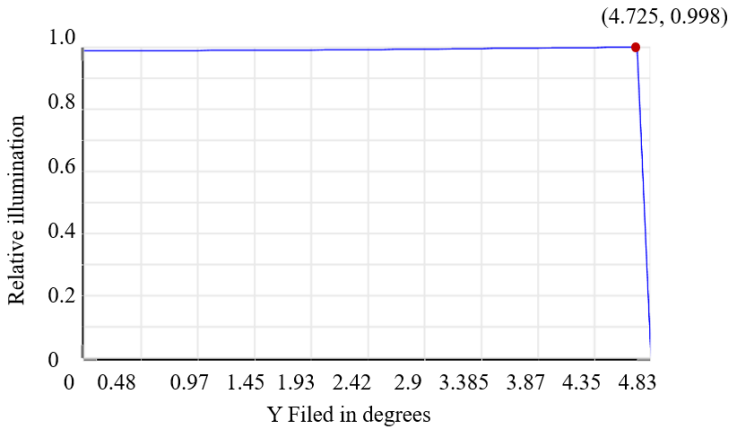

Figure 9. Relative illumination of the imaging system.

 doi:10.20944/preprints202603.0912.v1

Table 3. Key parameters of the imaging system.

Parameters	Data
F#	2.5
Focal Length	81.6 mm
Filed of View	4° × 6°
Entrance Pupil Diameter	16.3 mm
MTF	167.3 lp/ mm > 0.3

Field curvature and distortion, which do not degrade image quality but may cause displacement of the image points, are also critical metrics for optical system evaluation. As depicted in Figure 10, the maximum field curvature is 0.11 mm, and the maximum distortion is 0.64%. Both values are well controlled, indicating effective suppression of these aberrations. The final design ensures that the system delivers high resolution and minimal distortion across its operational field of view.

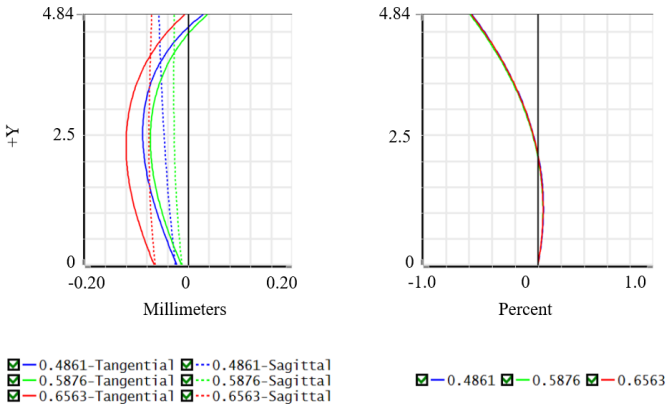

Figure 10. Field curvature/distortion of the detecting and imaging system.

3.2. Stray Light Analysis

As shown in Figure 7 (**b**), when all micromirrors of the DMD deflect by -12 degrees, no light in the entire system enters the detector for imaging. However, since ideal lenses do not exist in practice, it is necessary to conduct stray light analysis to verify the extent to which the system introduces stray light. The stray light analysis was performed on the detection and imaging system. The light source was configured as a uniform spot with a radius of 18 mm, operating at a laser wavelength of 588 nm and an output energy of 1 W. An aperture with an inner diameter of 24.3 mm was positioned in front of the lens assembly. A schematic of the stray light simulation setup is presented in Figure 11.

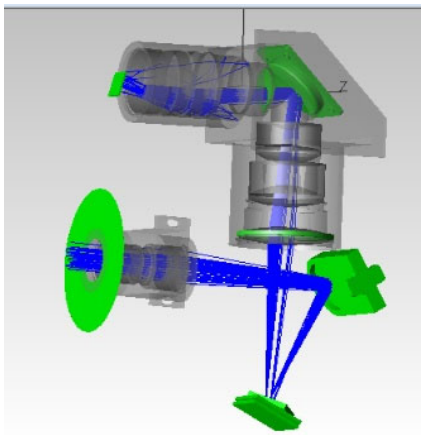

Figure 11. Schematic diagram of stray light simulation.

 doi:10.20944/preprints202603.0912.v1

The fields of view (FOVs) used in the analysis and the simulated optical power entering the system behind the aperture for each FOV is summarized in Table 4.

Table 4. Input optical power for different FOVs.

FOVs	X	Y	Input optical power /W
1	0	0	0.42948
2	0	2.5	0.46276
3	0	4.6	0.45166
4	4.6	0	0.45008
5	4.6	4.6	0.44869
6	-4.6	4.6	0.44849

Parameters of the optical lenses and mechanical structures are provided in Table 5.

Table 5. Key parameters of lenses and structural components.

Components	Reflectivity (%)	Transmittance (%)	Scattering rate (%)	Absorptivity (%)
Mirror	98.5	0	0.5	1
Lens	0.1	99.5	0.3	0.1
Struct	0.27	0	14.73	85

The DMD measures 25 × 25 mm and comprises 1000 × 1000 micromirrors. It is important to note that discrepancies between the simulation model and the actual DMD structure may introduce certain errors in the results. Analysis indicates that when the MEMS tilt angle is set to –12°, only laser light from Field of View 1 and Field of View 2 reaches the detector surface. The stray light energy distribution on the detector is illustrated in Figure 12.

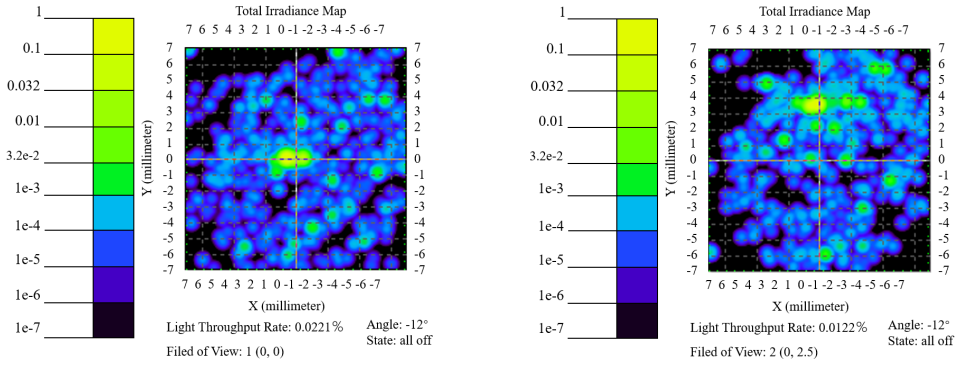

(**a**) (**b**)

Figure 12. Total stray light energy on the detector: (**a**) Field of View 1; (**b**) Field of View 2.

As shown in Figure 12 (**a**) and Figure 12 (**b**), the stray light is relatively dispersed across various fields of view. Specifically, the Light Throughput Rate is 0.0221% for Field 1 and 0.0122% for Field 2. And the energy distribution of the resulting stray light is illustrated in Fig. 13. As depicted in Figure 13 (**a**) and Figure 13 (**b**), the Light Throughput Rate is 0.0216% for Field 1 and 0.0119% for Field 2. This suggests that the stray light introduced by the DMD is of a very small order of magnitude.

 doi:10.20944/preprints202603.0912.v1

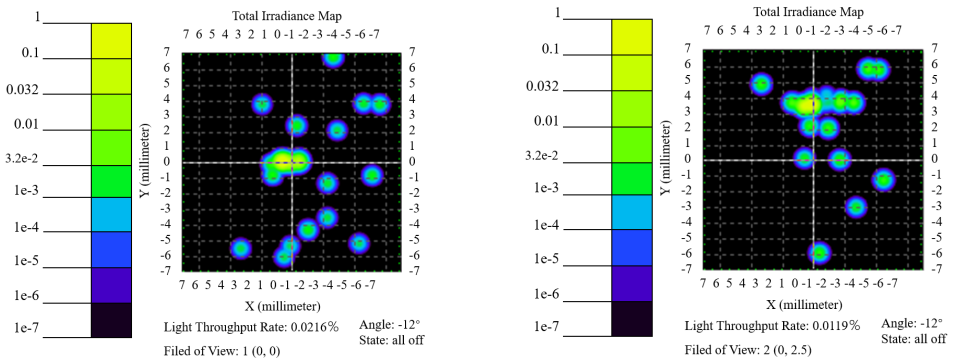

(**a**) (**b**)

Figure 13. Stray light energy distribution caused by protective window: (**a**) Field of View 1; (**b**) Field of View 2.

4. Experimental and Resulting

Based on the analysis results, a prototype was fabricated, and the integration and assembly of the optical system and control system were completed, as shown in Figure 14. Figure 14 (**a**) presents the front view of the system, Figure 14 (**b**) shows the internal structure of the system, where the control system comprises a DLP control board and an FPGA, and DMD is embedded in the optical system. Field experiments were conducted to assess the optical performance of the DMD-based anti-strong light imaging system designed to suppress strong light interference. The experimental setup is illustrated in Figure 15.

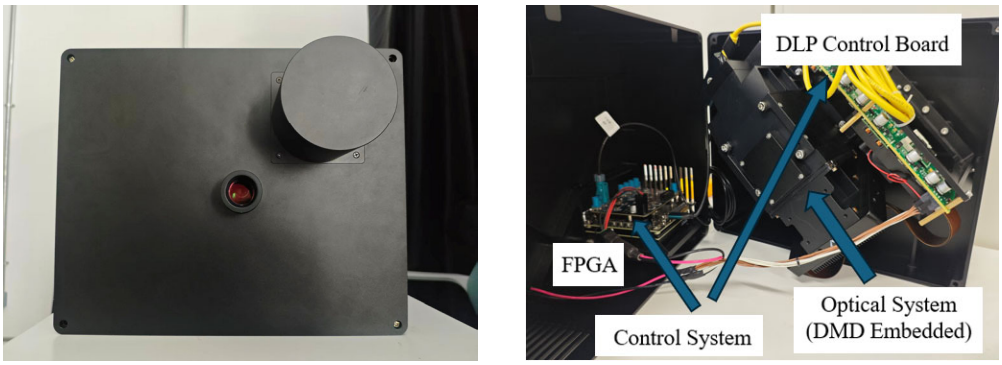

(**a**) (**b**)

Figure 14. Structure of the imaging system prototype: (**a**) Front view; (**b**) Internal structure.

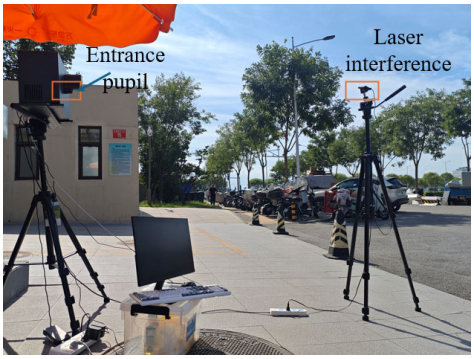

Figure 15. Experimental equipment.

 doi:10.20944/preprints202603.0912.v1

Imaging tests were performed on a target located 1 km away. A comparison between the image captured by the proposed system and that from a 60-megapixel smartphone is presented in Figure 16, showcasing the superior clarity and image quality of the designed optical system. It is worth noting that, compared with mobile phones or cameras, the images captured by this system are mirror images of the actual scenes.

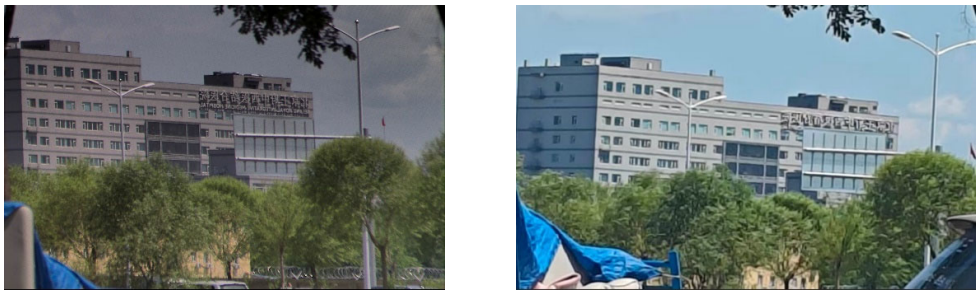

(**a**) (**b**)

Figure 16. Performance comparison of the imaging system: (**a**) Imaging system imaging; (**b**) Smartphone imaging.

To evaluate the strong light suppression capability, an interfering laser operating at a wavelength of 520 nm was positioned 5 meters from the entrance pupil of the imaging system, fully filling the entrance pupil. The people and buildings in the scene are located 70 meters away from the detector. The imaging performance of the detector, both before and after laser interference suppression and before and after algorithm processing, is shown in Figure 17.

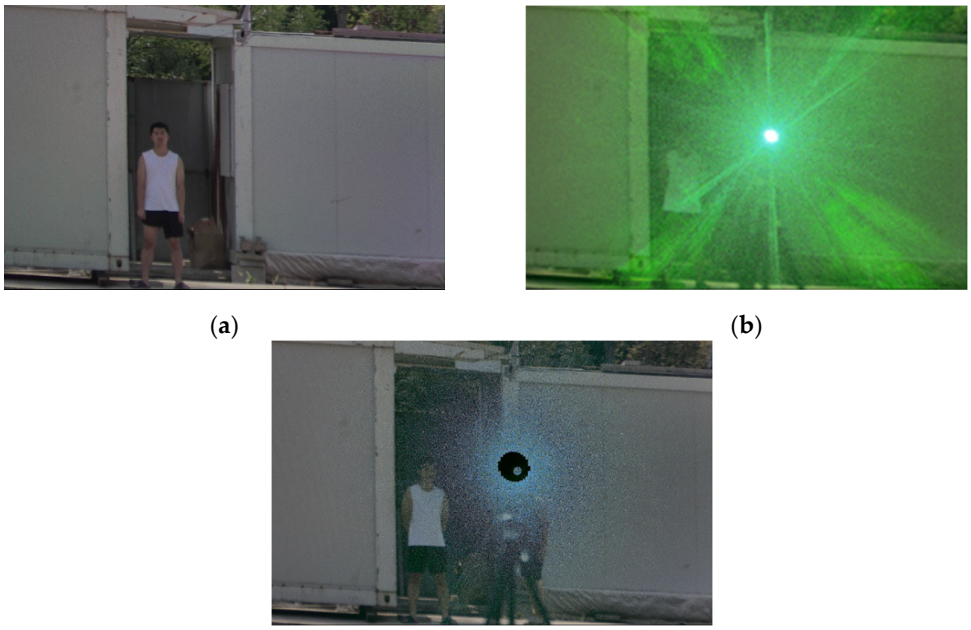

(**a**) (**b**)

(**c**)

Figure 17. Imaging performance before and after laser interference suppression: (**a**) Original imaging; (**b**) Before suppression (4.68×10^{-4} mW/cm^2); (**c**) After suppression.

The original scene is depicted in Figure 17 (**a**). Under laser interference, the imaging performance of the detector is shown in Figure 17 (**b**), where a bright spot appears at the center of the interfering laser. Strong glare effects spread outward from this spot, accompanied by radial glare streaks,

 doi:10.20944/preprints202603.0912.v1

significantly obscuring the background information. The power density of the laser interference at the entrance pupil is 4.68×10^{-4} mW/cm², at which point the glare nearly fills the entire frame.

After laser interference suppression by DMD regional flipping and imaging processing, the detector's imaging is shown in Figure 17 (**c**). The brightness of the interfering laser spot is greatly reduced, and the energy entering the detector is substantially diminished. Meanwhile, the glare in the image is significantly weakened, allowing for clear visibility of the background and figure.

5. Discussion

In this study, a DMD-based anti-strong-light detecting and imaging system was developed. A high-quality and compact secondary imaging optical system was designed, and the DMD was placed at the primary image plane to ensure precise laser suppression during DMD deflection. Furthermore, a prototype integrating the control system, imaging system, and glare suppression execution system was developed and manufactured. Finally, experiments were carried out to verify the glare suppression performance of the detection system.

Compared with Ref. [15], our prototype can achieve active strong light suppression without shutting down the shutter, which guarantees that the detection system can continuously output images under strong light interference. In contrast to Refs. [23,24], the optical design in this study is simpler and has stronger spectral adaptability.

However, as shown in Chapter 4, during the experiments, when strong light was directly incident on the image, the stray light introduced by the system severely affected image observation: even though the power of stray light is theoretically much lower than that of the laser core, large green spots still appeared in the images.

The possible reasons are as follows:

1. The sources of stray light may be more extensive: the laser emits from the fiber aperture with inherent diffraction effects; in the enclosed prototype, light may undergo multiple reflections among the prototype housing, imaging lenses, and DMD, and such a complex process is difficult to simulate and calculate.

2. Lasers have excellent monochromaticity, and the visual effect caused by the same light intensity is stronger than that of sunlight.

3. The DMD has a complex structure, which includes not only millions of micromirrors but also structures such as hinges and gaps, making accurate modeling difficult to implement.

Therefore, we must point out the following limitations of this study: we only analyzed the stray light potentially introduced by the system at the geometrical optics level, without considering the diffraction effects that may accompany the laser emission from the optical fiber. Meanwhile, due to the functional limitations of the software, the operating state of regional DMD flipping mentioned in this work was not analyzed; instead, only a simple overall DMD deflection of −12° was adopted. The insufficiently precise modeling of the DMD may also lead to deviations between simulations and experiments. Although this does not affect the authenticity of the data in this paper, it limits the guidance of the simulation and experimental results for practical applications.

6. Conclusions

This study successfully designed, optimized, and experimentally validated a DMD-based anti-strong-light detection and imaging system, specifically tailored for long-distance applications. The optical architecture presented integrates a long-focal-length objective, which provides an extensive depth of field crucial for remote sensing. A key feature of the system is an off-axis relay system incorporating a deliberately tilted image plane. This configuration effectively corrects aberrations, particularly those introduced by the DMD's non-planar operation, ensuring precise pixel-to-pixel correspondence between the DMD and the detector for accurate strong light suppression. Optical simulations confirmed robust imaging performance, with a MTF value exceeding 0.3 at 167.3 lp/mm across the full field of view. Experimental validation demonstrated the system's capability to clearly

 doi:10.20944/preprints202603.0912.v1

image scenes at 1 km while effectively mitigating laser interference by dynamically redirecting incident light, thus preventing sensor saturation. This research provides a robust, high-performance solution that significantly enhances imaging capabilities in challenging, glare-intensive environments, making it highly suitable for applications in surveillance, autonomous navigation, and remote sensing.

Author Contributions: Conceptualization, Z.T. and Y.M.; methodology, Z.T. and X.W.; software, B. Z.; validation, Z.T., X.W., Y. M. and B. Z.; formal analysis, R. Z.; investigation, H. C. and C. Y.; resources, L. X.; data curation, Z.T.; writing—original draft preparation, Z.T.; writing—review and editing, L. X.; visualization, H. C.; supervision, L. X.; project administration, L. X.; funding acquisition, L. X. All authors have read and agreed to the published version of the manuscript.

Funding: This research was funded by Enterprise Innovation and Development Joint Fund of the National Natural Science Foundation (Grant No. U24B2009).

Institutional Review Board Statement: Not applicable.

Informed Consent Statement: Not applicable.

Data Availability Statement: The data presented in this study are available in the article.

Conflicts of Interest: The authors declare no conflicts of interest.

References

1. Song Z., Jiang H., Lin H., et al., A high dynamic range structured light means for the 3D measurement of specular surface. *Opt. Lasers Eng* **2017**, 95, 8-16. [https://doi.org/10.1016/j.optlaseng.2017.03.008].
2. Guan X., Qu X., Niu B., et, al., Pixel-level mapping method in high dynamic range imaging system based on DMD modulation. *Opt. Commun* **2021**, 499 127278. [https://doi.org/10.1016/j.optcom.2021.127278].
3. Liu Z., Li M., Lu X., et, al., On-machine detection technology and application progress of high dynamic range fringe structured light. *CHIN OPT* **2024**, 17, 1-18. [https://doi.org/10.37188/CO.2023-0068].
4. Hong L., Hu C., Liu Y., et al., 350-2500 nm supercontinuum white laser enabled by synergic high-harmonic generation and self phase modulation. *PhotoniX* **2023,** 4, 11. [https://doi.org/10.1186/s43074-023-00088-2].
5. Cao S., He Y., Wang J., et al., Development Status of High Energy Laser Protection Technology for Satellites. *Vacuum And Cryogenics* **2024**, 30, 1-9. [https://doi.org/10.12446/j.issn.1006-7086.2024.01.001].
6. Jiang Y., Liu H., Wang L., et al., Design and preparation technology of laser protective film window of satellite. *CHIN OPT* **2019**, 12, 804-809. [https://doi.org/10.3788/CO.20191204.0804].
7. Zheng J., Li Z., Zhang M., et al., New type of coatings combining invisibility and high power laser protection function. *Ceram. Int* **2024**, 50, 11442-11450. [https://doi.org/10.1016/j.ceramint.2024.01.044].
8. Zhu J., Ma Z., Gao L., et al., Reflective laser protective coating based on plasma spraying. *CHIN OPT* **2017**, 10, 578-587. [https://doi.org/10.3788/CO.20171005.0578].
9. Li R., Xing Y., Zhang Z., et al., Process Study of Plasma Sprayed YSZ Thermal Barrier Coatings. *Surf. Technol* **2024**, 53, 217-229. [https://doi.org/10.3390/coatings14050626].
10. Zhu J., Ma Z., Gao L., et al., Influence of microstructure on the optical property of plasma-sprayed Al, Cu, and Ag coatings. *Mater. Des* **2016,** 111,192-197. [https://doi.org/10.1016/j.matdes.2016.08.090].
11. Wang Z., Ji X., Dong N., et al., Femtosecond laser-induced phase transition in VO_2 films. *Opt. Express* **2022**, 30, 47421-47429. [https://doi.org/10.1364/OE.477910].
12. Tongazzi A., Gandolfi M., Li B., et al., Opto-thermal dynamics of thin-film optical limiters based on the VO2 phase transition. *Opt. Mater. Express* **2023**, 13, 41-52. [https://doi.org/10.1364/OME.472347].
13. Liu Q., Hu S., Zhang C., et al., Polarization-dependent and wavelength-tunable optical limiting and transparency of multilayer selenium-doped black phosphorus. *Adv. Opt. Mater* **2021,**9, 2001562. [https://doi.org/10.1002/adom.202001562].
14. Liu Z., Lu Y., Hou D. Research progress of VO_2 thin film as laser protecting material. *Proc. SPIE 10710, Young Scientists Forum 2017*, Shanghai, China, 107100O (5 March 2018). [https://doi.org/10.1117/12.2310075].

 doi:10.20944/preprints202603.0912.v1

15. Bateman A. Mutually assured surveillance at risk: Anti satellite weapons and cold war arms control. *J Strategic Stud* **2022,** 45, 119-142. [https://doi.org/10.1080/01402390.2021.2019022].
16. Ye Q., Wu Y., Li Y., et, al., A Retroreflection Reduction Technique Based on the Wavefront Coded Imaging System. *Crystals* **2021,** 11, 1366. [https://doi.org/10.3390/cryst11111366].
17. Wang L., Dou X., Ye Q., et, al., Wavefront coded light-field imaging system to achieve substantial retroreflection reduction and anti-laser blinding property. *Optik* **2019,** 192, 162947. [https://doi.org/10.1016/j.ijleo.2019.162947].
18. Yang Z., Wang P., Li X., et, al., 3D laser scanner system using high dynamic range imaging. *Opt. Lasers Eng* **2014,** 54, 31-41. [https://doi.org/10.1016/j.optlaseng.2013.09.003].
19. Wu, L., Wang, X., He, X., et, al., Arbitrary Multiple Beam Forming by Two Cascaded Liquid Crystal Optical Phased Arrays. *Opt. Express* **2018**, 26, 17066-17077. [https://doi.org/10.1364/OE.26.017066].
20. Wu, J., Feng, T., Chen, Q., et al., Photoacoustic guided wavefront shaping using digital micromirror devices. *Opt. Laser Technol* **2024**, 174, 110570. [https://doi.org/10.1016/j.optlastec.2024.110570].
21. Ryoo, H., Dong, W., Hahn, J. Analysis of the effective reflectance of digital micromirror devices and process parameters for maskless photolithography. *Microelectron. Eng* **2011**, 88, 235-239. [https://doi.org/10.1016/j.mee.2010.10.039].
22. Zhou, J., Qiao, Y., Sun, Z., et, al., Design of a dual DMDs camera for high dynamic range imaging. *Opt. Commun* **2019**, 452, 140-145. [https://doi.org/10.1016/j.optcom.2019.07.008].
23. Ritt, G., Schwarz, B., Eberle, B. Preventing image information loss of imaging sensors in case of laser dazzle. *Opt, Eng*. **2019,** 58, 013109. [https://doi.org/10.1117/1.OE.58.1.013109].
24. Ritt, G., Eberle, B. Use of complementary wavelength bands for laser dazzle protection. *Opt, Eng* **2020,** 59, 015106. [https://doi.org/10.1117/1.OE.59.1.015106].
25. Sun, Y., Hu, Y., Wang, Y., et, al., Analysis on Aberration of Digital Micromirror Device in Convergent Imaging Path. *Acta Optica Sinica* **2019,** 39, 144-149. [10.3788/AOS201939.0311001].